On the occurrence of postmidnight equatorial *F* region irregularities during the June solstice

Guozhu Li,[1] Baiqi Ning,[1] M. A. Abdu,[2] Xinan Yue,[3] Libo Liu,[1] Weixing Wan,[1] and Lianhuan Hu[1]

Received 26 August 2010; revised 26 December 2010; accepted 24 January 2011; published 22 April 2011.

[1] Postmidnight equatorial *F* region irregularities (EFIs) are known to develop mainly during the solstitial months. However, it is not well understood whether they occur at all longitudes and what process causes their occurrence at different longitude sectors. In this study, we use the GPS total electron content (TEC) fluctuations obtained from a global GPS network and spread *F* in ionograms from Jicamarca (283°E, 12°S, Dip 1°N) in the American longitude sector and Kwajalein (167°E, 9°N, Dip 4°N), Bac Lieu (106°E, 9°N, Dip 2°N), and Chumphon (99°E, 11°N, Dip 3°N) in the Pacific and Asian longitude sectors during 2000–2009, to investigate the EFI characteristics during June solstice. Results from global TEC fluctuations show that at solar maximum, the occurrence rate of postmidnight EFIs is high in African and Pacific regions, moderate in the Southeast Asian region, and low in the Peruvian region and that most postmidnight EFIs are the continuation of postsunset EFIs. During solar minimum the postmidnight EFIs were rarely observed in TEC but were very frequent in ionograms. The latter had more frequent postmidnight onsets over Peru, whereas they were initiated during late postsunset hours in Pacific and Southeast Asian longitudes. In both longitudes the postsunset layer rise occurred with some delay. The layer rise was more prominent on spread *F* nights over Jicamarca and less so over Pacific longitudes. The results showing different degrees of association at the different longitudes between the postsunset/postmidnight EFIs and *F* layer heights highlight the influence of other factors in the late-night EFI development. Perturbation seeds and plasma drifts/neutral winds, in particular, are discussed as strong candidates for causing these irregularities in the June solstitial months of solar minimum years.

Citation: Li, G., B. Ning, M. A. Abdu, X. Yue, L. Liu, W. Wan, and L. Hu (2011), On the occurrence of postmidnight equatorial *F* region irregularities during the June solstice, *J. Geophys. Res.*, *116*, A04318, doi:10.1029/2010JA016056.

1. Introduction

[2] Equatorial *F* region irregularities (EFIs) have been extensively studied through multi-instrument observations, such as diffuse echoes in ionograms, backscatter plumes in VHF radar echoes, total electron content (TEC) bite-outs, and pronounced density depletions from in situ satellites [e.g., *Woodman and LaHoz*, 1976; *Abdu et al.*, 1981; *Sripathi et al.*, 2008; *Basu et al.*, 2009; *Kil et al.*, 2009]. From these investigations it is known that most EFIs initiate at postsunset hours and continue to midnight, with the occurrence rate peaking during premidnight hours and decreasing steadily during the rest of the night. Although, from case studies, the EFIs are found to occur also during postmidnight hours, they are generally much weaker and much less frequent than the postsunset events. However, from an examination of the ionograms recorded at Fortaleza, *MacDougall et al.* [1998] reported a secondary maximum occurrence of EFIs at postmidnight/presunrise hours. Such EFIs took the form of patches with eastward velocities of about 50 m s^{-1}. In the Indian sector, the peak occurrence of EFIs during postmidnight hours has been observed preceded by an abnormal increase of *F* region height during the June solstice of solar minimum [*Sastri et al.*, 1979]. Recently, using the Communications/Navigation Outage Forecasting System (C/NOFS) satellite in situ observations, *Huang et al.* [2010] found frequent occurrence of solar minimum EFIs in the midnight to dawn sector. Such kinds of EFIs appear to be different from the decaying EFIs which are initiated during postsunset hours or that associated with the postmidnight frequency-type spread *F* in ionograms. The drift velocities were found to be upward and westward and reached 200–400 m s^{-1}, which indicates that these postmidnight EFIs are active and still growing.

[3] It is generally accepted that the Rayleigh-Taylor (R-T) instability mechanism is responsible for the generation and growth of the EFIs. The growth rate of the R-T instability

[1]Beijing National Observatory of Space Environment, Institute of Geology and Geophysics, Chinese Academy of Sciences, Beijing, China.
[2]Divisão de Aeronomia, Instituto Nacional de Pesquisas Espaciais, São Paulo, Brazil.
[3]University Corporation for Atmospheric Research, Boulder, Colorado, USA.

0148-0227/11/2010JA016056

depends on the external driving forces, such as neutral wind, electric and magnetic fields, together with background ionospheric properties, for example, the flux tube integrated Pedersen conductivity and upward plasma density gradients [e.g., *Sultan*, 1996; *Abdu*, 2001]. The postsunset EFIs are generally thought to be associated with the evening pre-reversal enhancements (PRE) of vertical drift velocity [*Fejer et al.*, 1999]. Under the action of the PRE, the ionosphere is rapidly elevated to higher altitudes, where collision frequencies are low, favoring the growth of the irregularities by the R-T instability mechanism. The postmidnight EFIs are mainly due to either the passage of fossil plumes generated elsewhere since EFIs can drift eastward or westward [*MacDougall et al.*, 1998; *Bhattacharyya et al.*, 2001], that is, the continuation of the generation and dynamics of the postsunset irregularities, or the irregularities freshly generated at postmidnight hours owing to local plasma instabilities. From an investigation of spread *F* at Trivandrum, *Subbarao and Krishnamurthy* [1994] reported that the shift in peak occurrence of spread *F* from postsunset to postmidnight hours can be accounted for by the R-T instability mechanism. They suggested that the increase in *F* layer height, which precedes the postmidnight onset of spread *F*, can render the *F* region unstable to the combined effects of the cross-field and the gravitational terms in the R-T instability growth rate. Later, using the ionogram data obtained at Kodaikanal, *Sastri* [1999] reported that the increase in *F* layer height is not a sufficient condition for the postmidnight onset of spread *F*. Note that the spread *F* presented in the work of *Sastri* [1999] is mostly frequency-type spread *F*. Moreover, using the Gadanki radar observations, *Patra et al.* [2009] investigated the low-latitude *F* region field-aligned irregularities (FAIs) during July–August 2008 and found that the FAI echoes were observed on all 20 nights of radar observations and were mostly confined to the postmidnight hours.

[4] Although many studies on postmidnight EFIs have been performed in the Indian and Brazilian longitude regions, there are still some open questions on whether the postmidnight EFIs occur at all longitudes and what processes trigger the their development at different longitudes during the June solstice of solar minimum. Interestingly, from the recent C/NOFS satellite observations, *Huang et al.* [2010] presented some cases of postmidnight EFIs, and they raised several unresolved questions about the generation of postmidnight plasma bubbles. In the present study, we use the GPS TEC fluctuations obtained from a global GPS receiver network and ionosonde spread *F* measured at four selected stations, during 2000–2009, to get the occurrence probability of postmidnight EFIs during the June solstice. In the case of the ionosonde-recorded spread *F*, we only consider the range-type spread *F* (that do not include the convecting patches from elsewhere) to investigate the localized process triggering the development of the postmidnight EFIs on geomagnetic quiet days (defined by a daily averaged *Kp* value less than 3).

2. Data Selection and Processing

[5] Ground-based GPS TEC and ionograms provide the most abundant data of ionospheric irregularities, which have been extensively used to study the occurrence characteristics of the EFIs [e.g., *Nishioka et al.*, 2008; *Abdu et al.*, 2009a; *Lee et al.*, 2009]. In this study, we use the TEC data from the International Global Navigation Satellite System Service (IGS) GPS receivers at equatorial latitudes to measure the TEC fluctuation index [*Pi et al.*, 1997], and obtain the post-sunset and postmidnight occurrence rate maps, the onset time and duration of EFIs in a manner similar to that considered by *Li et al.* [2009a, 2009b]. Briefly, within a grid of 5° in geographical longitude and 1° in latitude (locations of ionosphere penetration points at 400 km altitude), the number of samples with the rate of TEC change index (ROTI) higher than 0.075 TECU min^{-1} [*Nishioka et al.*, 2008] is divided by the total number of ROTI samples, to obtain the occurrence rate map in that square area at postsunset and postmidnight hours. If there are two ROTI values greater than 0.075 TECU min^{-1} within 1 h for a single GPS satellite, it is regarded as an EFIs event, and the time will be attributed to the onset time of the EFIs. Therefore the duration can be estimated from the onset and elapse times of the EFIs. The locations of the selected GPS TEC receivers are superposed as bold dots in Figure 3c.

[6] Ionosonde data are obtained from the stations Jicamarca (283°E, 12°S, Dip 1°N), Kwajalein (167°E, 9°N, Dip 4°N), Bac Lieu (106°E, 9°N, Dip 2°N), and Chumphon (99°E, 11°N, Dip 3°N), which are located in the Peruvian, Pacific, and Southeast Asian sectors, respectively. Figures 1a and 1b show two typical spread *F* ionograms obtained from Jicamarca. It may be noted that the irregularities first appeared in the lower part of the bottomside *F* region, and then extended to the *F* layer peak. *Chen et al.* [2006] defined the two kind of spread *F* as range-type spread *F*–I (RSF–I) and RSF–II. In the following statistics of spread *F*, only these two types of spread *F* will be considered, since the frequency spreading type may simply be a decay product of range-type spread *F* [*King*, 1970]. The spread *F* type and the onset time and the duration of the spread *F* events in the present statistical study are determined manually.

3. Results

[7] Figures 1 and 2 present several examples of the EFIs observed by the Jicamarca ionosonde and the GPS receiver (AREQ) on geomagnetic quiet days (daily averaged $Kp < 1$). As shown in Figures 1c–1f, strong spread *F* irregularities were observed at premidnight and postmidnight hours on 25 August 2004 and 3, 27, and 30 August 2008, respectively. The spread echo in ionogram covers an altitude range of more than 200 km. The ROTI, slant TEC (STEC), and vertical TEC (VTEC) measurements during these days are shown in Figure 2. The VTEC is calculated from STEC by assuming a thin shell ionosphere at 400 km altitude [e.g., *Sripathi et al.*, 2008]. It is seen from Figure 2a that on 25 August 2004, the STEC and VTEC fluctuated rapidly (apparent "bite-out"), and ROTI values are higher than the threshold value of 0.075 TECU min^{-1} (marked as dashed line) during the period 0130–0630 UT, which corresponds to local premidnight and postmidnight hours (2100–0200 LT). However, when we note the TEC observations on 3, 27, and 30 August 2008, the ROTI values are always lower than 0.075 TECU min^{-1} and have no abrupt TEC fluctuations, whereas the ionosonde registered strong range-type spread *F*. It probably indicates that at solar minimum, there is remarkable difference in the relationship between TEC fluctuation (ROTI) and range spread *F* intensity during postmidnight hours. This difference cannot be attributed to a

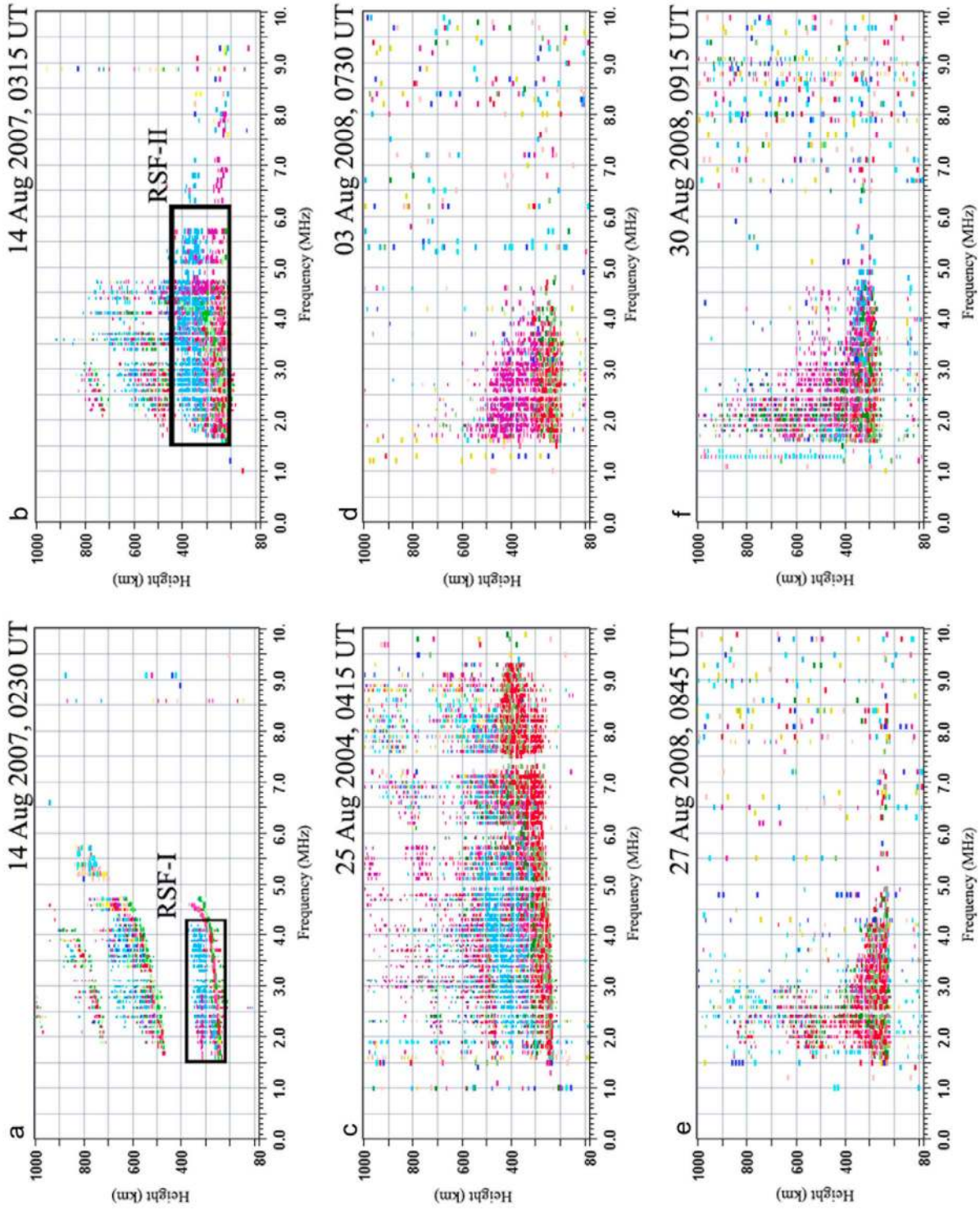

Figure 1. Examples of range-type spread *F* (RSF) recorded by Jicamarca ionosonde (283°E, 12°S, Dip 1°N). (a and b) RSF–I (0230 UT) and RSF–II (0315 UT) observed on 14 August 2007. (c–f) RSF that occurred at premidnight and postmidnight and that will be compared with simultaneous GPS total electron content (TEC) fluctuations (see Figure 2).

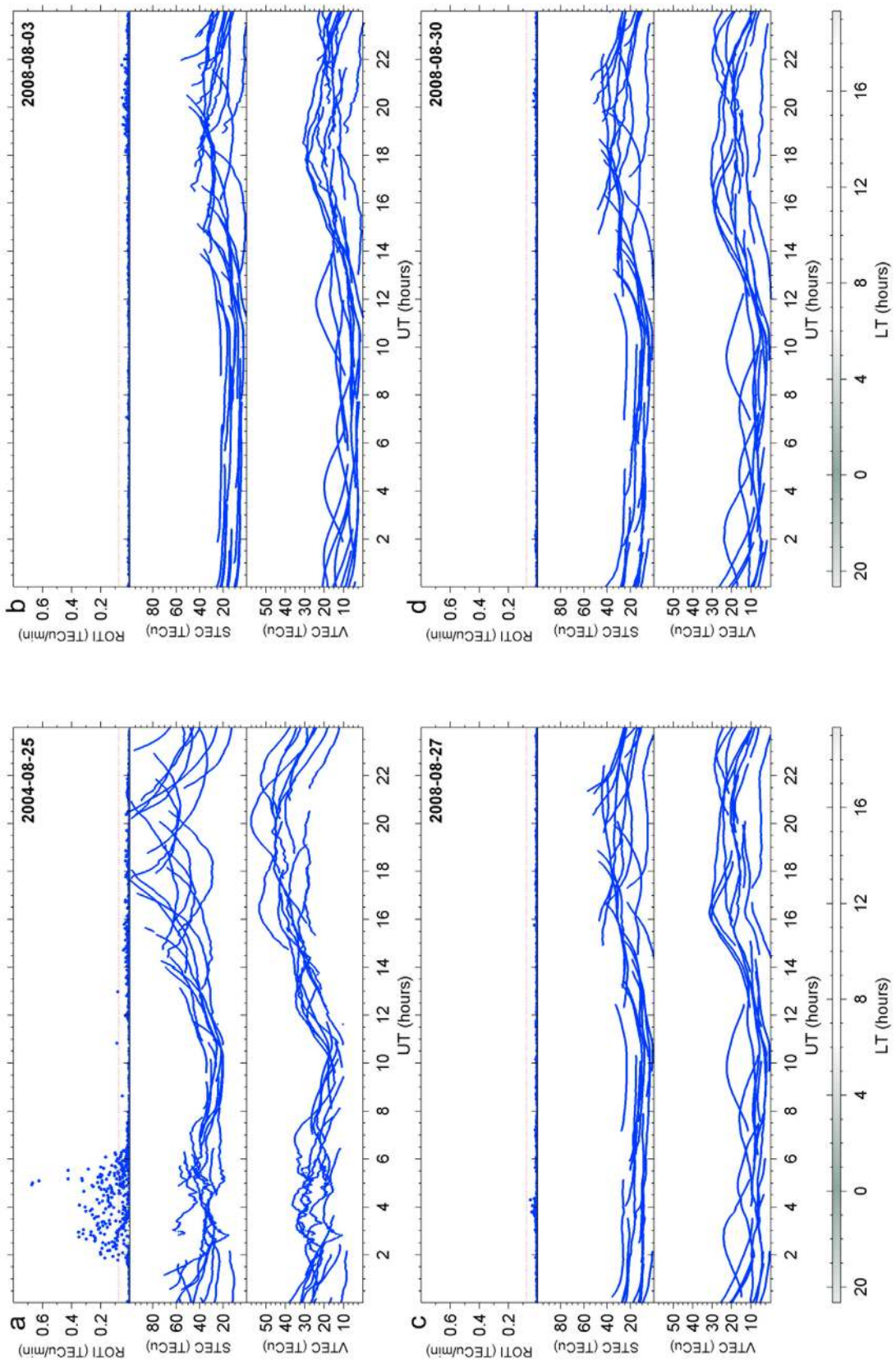

Figure 2. The rate of TEC change index (ROTI), slant TEC (STEC), and vertical TEC (VTEC) obtained from a GPS receiver located near Jicamarca for (a) 25 August 2004, (b) 3 August 2008, (c) 27 August 2008, and (d) 30 August 2008.

possibility that ROTI failed to record TEC fluctuations, since no apparent fluctuations can be found in the nighttime values of the STEC and VTEC in Figure 2. Possible implications of the difference will be discussed later in the statistical analysis of EFIs.

3.1. Occurrence Characteristics of the EFIs Obtained From GPS TEC Fluctuations

[8] Figure 3 is the map of occurrence rates for postsunset (Figure 3a) and postmidnight (Figure 3b) EFIs observed during the June solstice of the years 2000–2009. The corresponding solstitial average values of solar 10.7 cm flux ($F10.7$) are listed in Table 1. In Figure 3c, the differences in occurrence rates between postsunset and postmidnight hours are also shown. It is found that at solar maximum 2000–2002 (averaged $F10.7 \sim 150$), high occurrence rates of irregularities are present in the African (centered around 30°E) and Pacific (centered around 180°E) longitude regions, for both postsunset and postmidnight hours. The postsunset occurrence probability is apparently higher than that of postmidnight. In the Southeast Asian (centered around 120°E) longitude region, the occurrences of EFIs are moderate and mainly observed at postsunset hours. In contrast, in the Peruvian (centered around 290°E) longitude region, the occurrence rates are very low with the value <5%. During solar medium years 2003–2005 (averaged $F10.7 \sim 100$), the EFIs are found to predominantly occur in the African and Pacific longitude regions, with peak occurrence rates located at postsunset. However, for solar minimum years 2006–2009 (averaged $F10.7 \sim 70$), except African sector, the EFIs (seen from TEC fluctuations) are absent at other longitude regions.

[9] Using in situ satellite observations, the global longitudinal and seasonal distribution of EFIs and *F* region vertical drifts has been investigated by many researchers [e.g., *Fejer et al.*, 1999; *Oyekola et al.*, 2007; *Oyekola*, 2009]. Two peaks of EFIs are reported in the June solstitial months at longitude sectors of Atlantic-African and Pacific [e.g., *Kil et al.*, 2009]. In general, the present longitudinal distribution of GPS TEC fluctuations at solar maximum and medium epochs agrees well with in situ satellite observations; the two sectors, African and Pacific, are very prone to the occurrence of EFIs during the June solstice, and the postmidnight EFIs occurrence probability is apparently lower than that of postsunset. On the other hand, in the Peruvian sector, the EFIs were totally suppressed. Although there are many studies on the global morphology of EFIs using in situ satellite observations, the onset time and duration distribution of EFIs have not been well studied, owing to the effects that the satellite cannot continuously observe at a fixed position and owing to an uncertainty to determine the onset time of the EFIs.

[10] In order to investigate whether the postmidnight EFIs are the continuation of postsunset EFIs or generated at postmidnight hours, we plotted the onset time and duration distribution of EFIs obtained from ground-based GPS TEC fluctuations in Figure 4, for four selected stations located at equatorial latitudes around 15°E, 100°E, 185°E, and 290°E, respectively. The solid blue circle in Figure 4 indicates the onset time, and the bold green line marks the duration of EFIs. The data coverage is shown as vertical white (with data) and red (no data or daily averaged $Kp \geq 3$) bar at the left of each plot. The shaded area represents the local nighttime, and the vertical bold line at the bottom of each plot marks midnight. From Figure 4 we note that at solar maximum, most EFIs start growing at postsunset hours, around 2000 LT, and continue to occur for a long duration extending to the postmidnight hours and slowly decay by about 0300 LT. The distribution of onset time and duration indicates that most postmidnight EFIs of solar maximum are the continuation of postsunset EFIs in the African, Southeast Asian, and Pacific longitudes. During solar minimum years 2006–2009, the EFIs are mainly observed in the African sector, and they were generated during postsunset hours, and some of them continued to postmidnight hours with shorter duration as compared to those of solar maximum.

3.2. Occurrence Characteristics of the EFIs Observed Through Ionosonde Spread *F*

[11] Figure 5 shows the occurrence probability, the onset time, and the duration distribution of spread *F* over Jicamarca. At the bottom part of each plot, the percentage occurrence rate is shown at an hourly interval, which is obtained through the number of spread *F* days divided by the number of total days in each hour. The spread *F* onset time and duration are marked by the solid circle and bold lines, respectively. At solar maximum, the spread *F* occurrence probability is low, similar to the characteristics of the GPS TEC fluctuations observed in the 290°E sector of Figure 4. However, at solar minimum, the occurrence probability of spread *F* is observed with a value up to 50%, significantly higher than the occurrence rate of GPS TEC fluctuations. Using the Jicamarca ionosonde and the GPS receiver (AREQ) observations from April 1999 to March 2000, *Chen et al.* [2006] performed a comparison between the GPS phase fluctuations and ionosonde spread *F*. The results indicated that the occurrence statistics of GPS phase fluctuations is similar to that of the ionosonde spread *F*. A lower occurrence rate of range-type spread *F* (less than 10%) was reported during the June solstice of solar maximum. Here the observations of spread *F* and TEC fluctuations at solar maximum are similar to the results reported by *Chen et al.* [2006]. However, at solar minimum, significant difference exists between the statistics of the GPS TEC fluctuations and that of spread *F*, which will be discussed below. The results also show that the EFI occurrence rates (from ionosonde spread *F*) over Jicamarca have a significant negative correlation with solar flux during the June solstice. Such a negative dependence of EFIs on solar flux has been reported also over the Indian longitude region. *Niranjan et al.* [2003], using the spread *F* observations at low-latitude station Waltair, investigated the postmidnight spread *F* occurrence probability and found that it is maximum during the June solstice months of low solar activity and decreased with an increase in the sunspot activity. At solar minimum, the onset of EFIs over Jicamarca mostly occurred during postmidnight hours. And the occurrence probability of the postmidnight EFIs is apparently higher than that of postsunset EFIs, with the peak occurrence rate centered around 0300 LT. The results indicate that the postmidnight spread *F* events of solar minimum years are predominantly initiated from local development during postmidnight hours, and not a continuation of postsunset EFIs. Inside such freshly generated postmidnight EFIs, the polarization electric field could be strong, consistent with C/NOFS observations as reported by *Huang et al.* [2010].

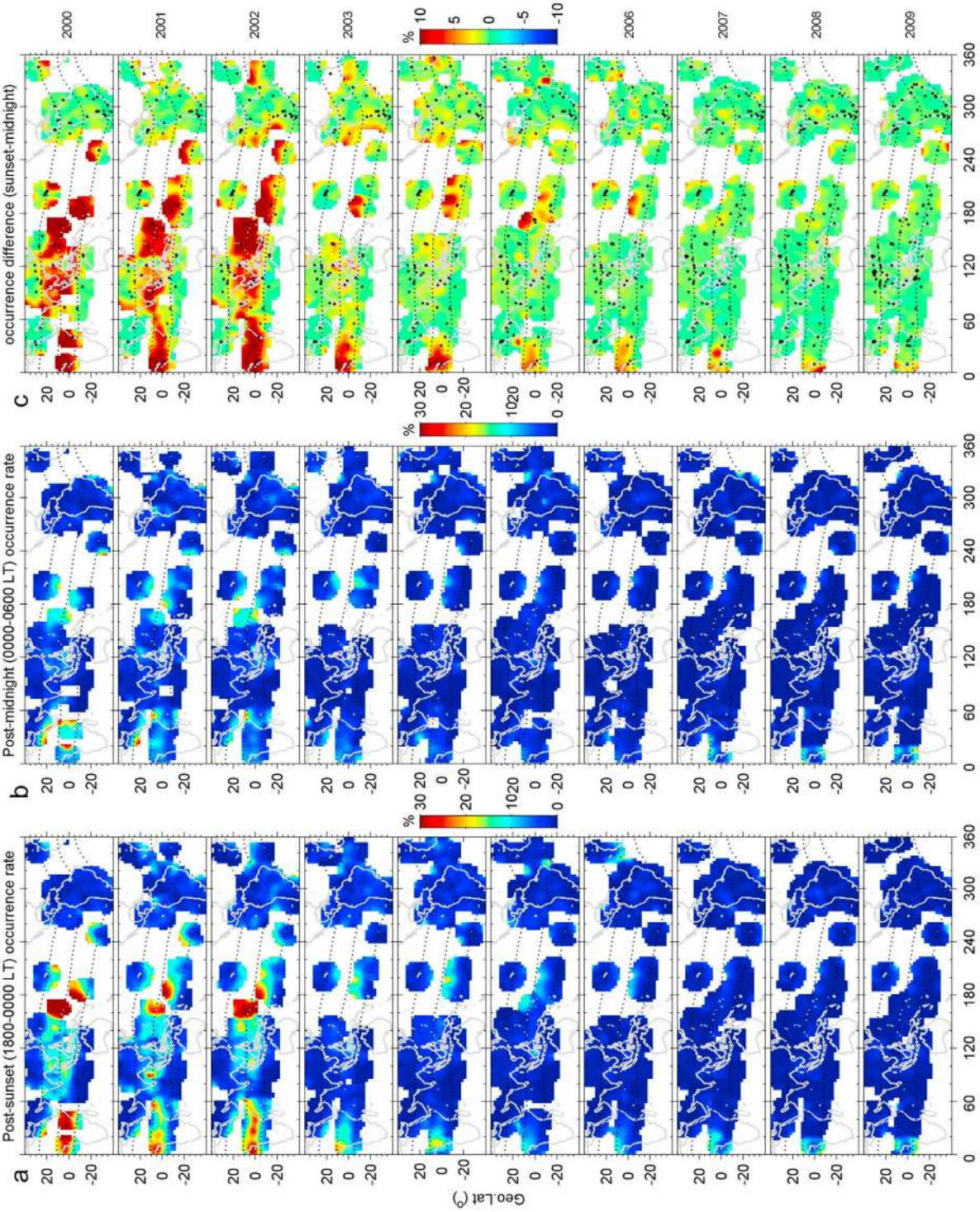

Figure 3. (a and b) The June solstitial EFIs' occurrence rates during the period of postsunset and postmidnight hours in 2000–2009. (c) The occurrence difference between postsunset and postmidnight, indicating that the postsunset EFIs' occurrence rate is apparently higher than that of postmidnight at solar maximum.

Table 1. Monthly Averaged Values of Solar 10.7 cm Flux (*F*10.7) During the June Solstice of 2000–2009

	2000	2001	2002	2003	2004	2005	2006	2007	2008	2009
May	189	151	182	119	102	102	83	76	70	72
June	186	179	153	133	101	97	79	76	68	71
July	211	136	179	132	122	100	78	74	68	70
August	167	167	188	125	113	93	81	71	68	69

[12] Figure 6 shows the spread *F* conditions observed at Kwajalein. We note that there are no data during the period of solar maximum and medium years 2000–2003 [*Reinisch et al.*, 2004]. But there appears to be little doubt that EFIs frequently occurred in this longitude at solar maximum, which can be seen from GPS TEC fluctuation and in situ satellite observations. As seen in Figure 6, in August 2004, spread *F* events started mostly during 1900–2000 LT and attained a peak occurrence before midnight. However, at solar minimum, most spread *F* initiated at premidnight hours around 2300 LT and had durations of more than 7 h extending to sunrise. The occurrence rate gradually reached up to about 80% around midnight. The rate of increase in the EFIs occurrence before the maximum and the decay rate are slow, except in years 2006–2007 when the decay rate after the maximum was much faster. Most postmidnight spread *F* irregularities are the continuation of those initiated during premidnight. Through a newly developed three-dimensional spread *F* model, *Huba et al.* [2008] investigated the evolution characteristics of irregularities and found that the growth time of the instability is about 15 min. There is a time delay of more than 1 h between the irregularities generation at the bottomside of *F* region and their rise to the topside. Since the spread *F* over Kwajalein was mostly initiated around 2300 LT and continued to sunrise hours, some of the events observed around 0200 LT might be still active and growing. The results for the Southeast Asian longitude are presented in Figure 7. Frequency modulated continuous wave (FMCW) ionosondes provided the ionograms over Chumphon and Bac Lieu since 2004. We utilized the data from both stations in this longitude because there is a large amount of data gaps for Bac Lieu and

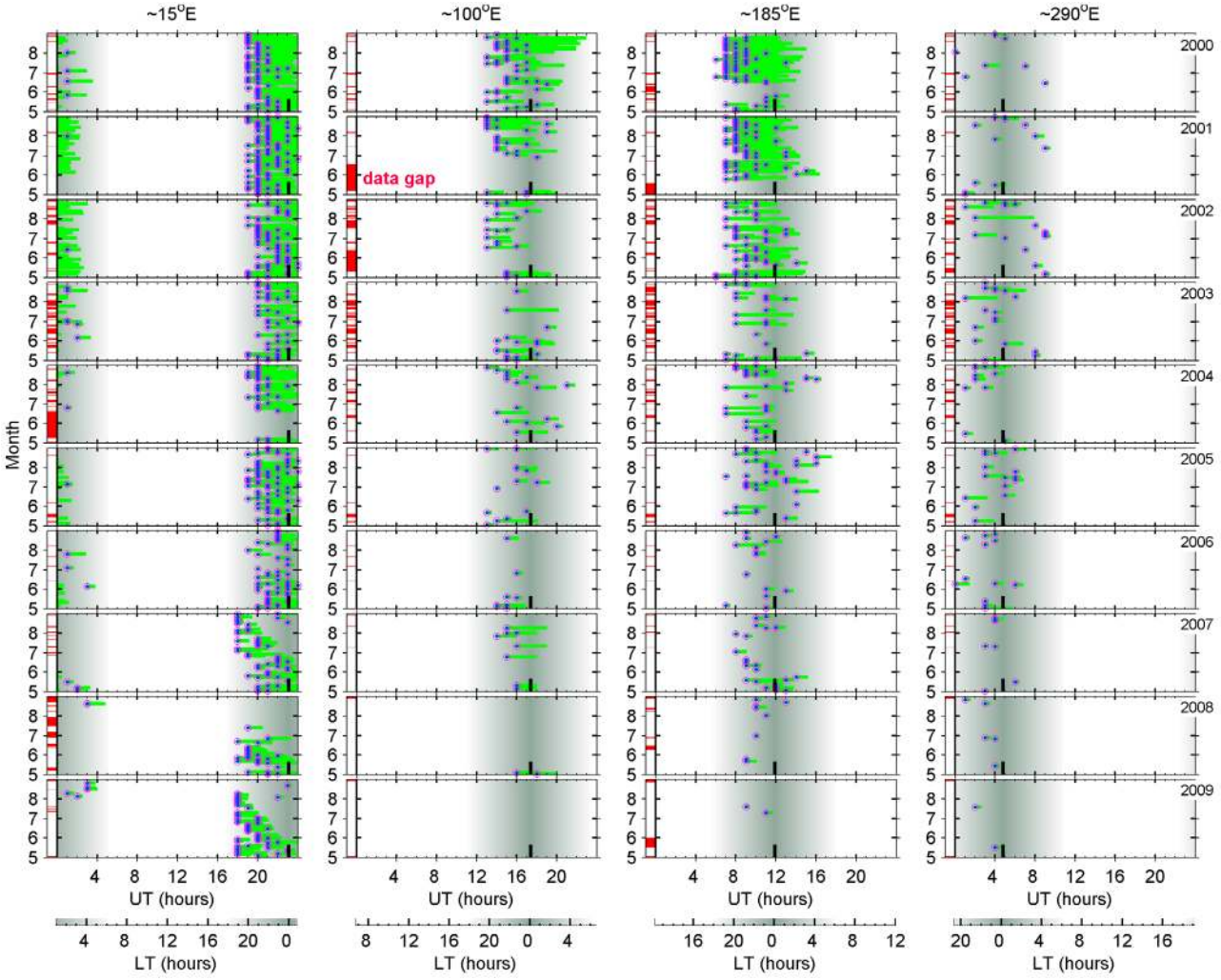

Figure 4. The onset time (shown as solid blue circle) and duration (bold green line) distribution of EFIs from GPS TEC fluctuations around 15°E, 100°E, 185°E, and 290°E during 2000–2009. The left vertical bar of each plot indicates the data coverage (red color means no data or daily averaged $Kp \geq 3$). The shaded area marks the local nighttime.

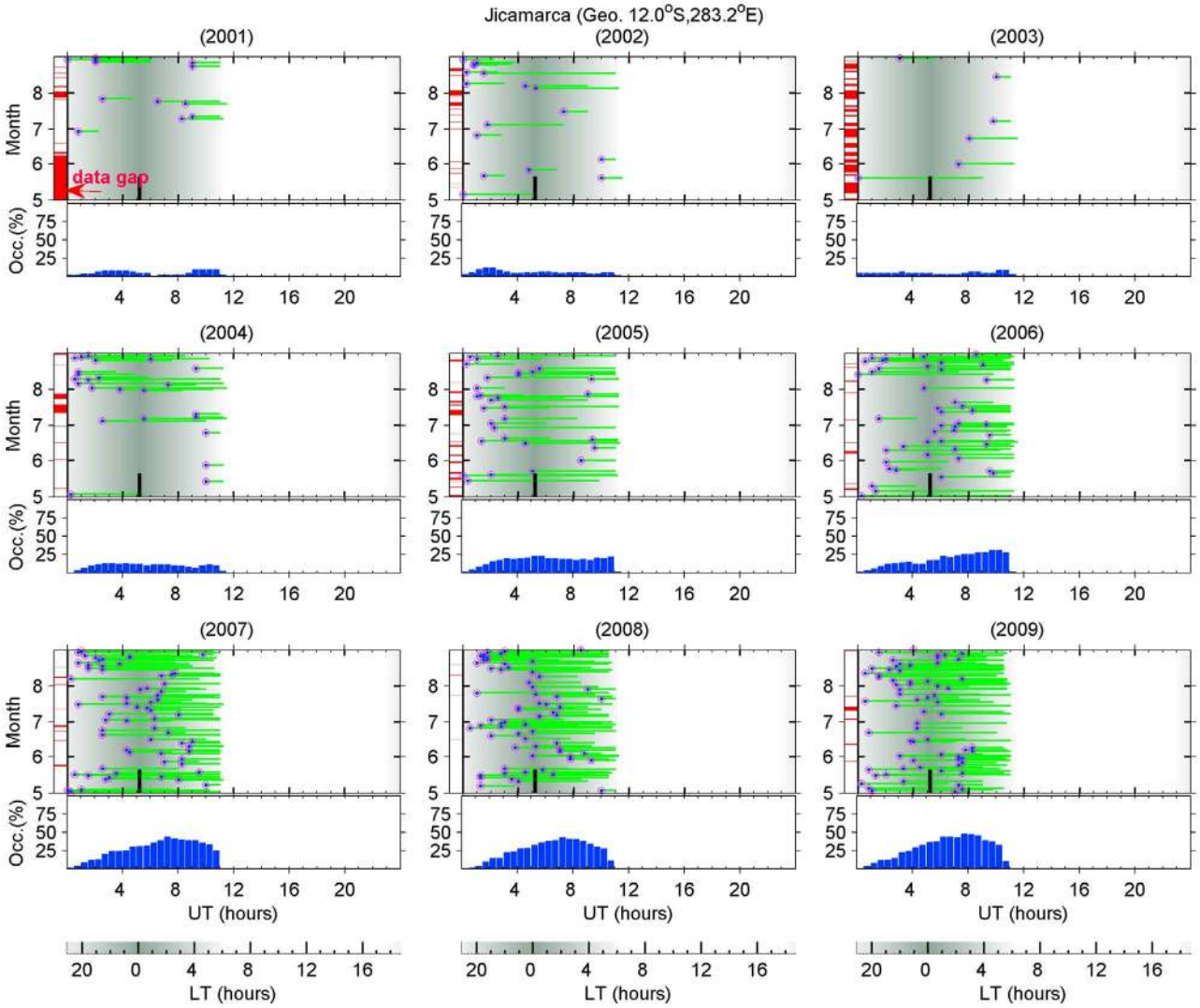

Figure 5. The onset time and duration distribution of spread *F* over Jicamarca during 2001–2009. The occurrence probability versus UT is shown at the bottom part of each plot.

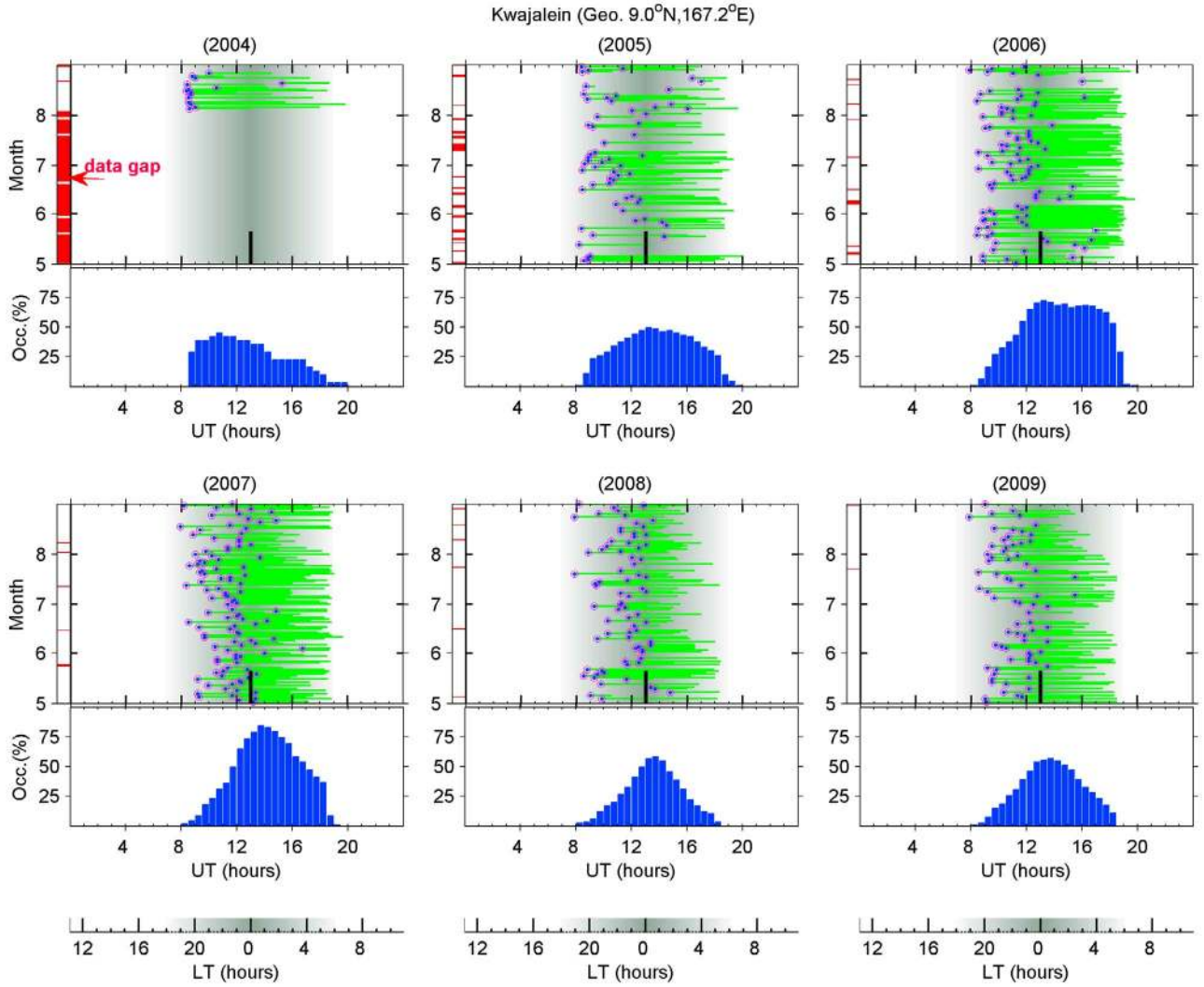

Figure 6. Same as Figure 5 but for Kwajalein (167°E, 9°N, Dip 4°N) spread *F* observations during 2004–2009.

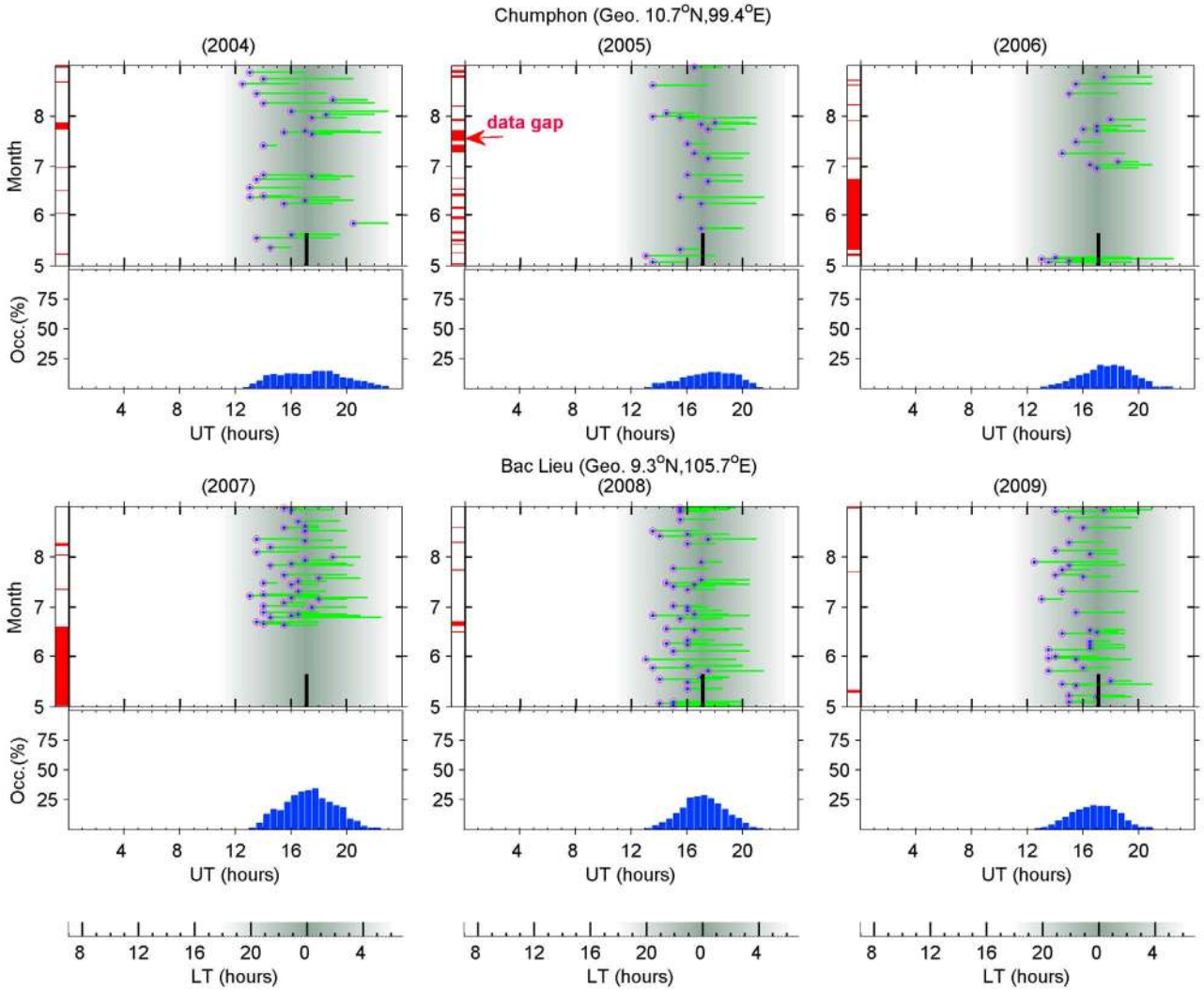

Figure 7. Same as Figure 5 but for Chumphon (99°E, 11°N, Dip 3°N) and Bac Lieu (106°E, 9°N, Dip 2°N) spread *F* observations during 2004–2009.

Chumphon, before and after 2006, respectively. Figure 7 shows that the spread *F* occurrence pattern in this sector is similar to that of Kwajalein. Spread *F* is initiated mainly during premidnight hours and lasts for several hours into postmidnight period. However, the peak occurrence probability of 30%, which is centered around midnight, is apparently lower than that of Kwajalein (80%). On the other hand, most spread *F* events last for only a short period of time, less than 5 h. Investigating the range-type spread *F* over Ho Chi Minh City, *Hoang et al.* [2010] presented an occurrence rate of 25% at ~2200 LT in the June solstice of solar maximum years (2002–2003). These results suggest that the spread *F* occurrence rate pattern in the Southeast Asian longitude is similar during solar maximum and minimum years except that the time of the peak occurrence rate shifted from postsunset hours during solar maximum to midnight hours during solar minimum.

4. Discussion

[13] In keeping with the findings from several cases of GPS TEC fluctuations and ionosonde spread *F* (see Figures 1 and 2), we note that a discrepancy exists between the statistical results of the EFIs occurrence shown in Figures 3 and 4 and Figures 5–7. At solar maximum, the TEC fluctuations and spread *F* show similar occurrence pattern, consistent with earlier studies [e.g., *Chen et al.*, 2006; *Lee et al.*, 2009]. However, at solar minimum the EFIs characterized by TEC fluctuations are rarely observed in Southeast Asian, Pacific, and Peruvian longitude regions, whereas the ionosonde spread *F* observations show a higher occurrence probability of EFIs, with values of 30%, 80%, and 50%, respectively. Such a contrasting feature could be partly due to the fact that the background density declined rapidly and attained a lowest value during the postmidnight hours of solar minimum. Therefore the absolute perturbation density is apparently lower than that of solar maximum and possibly cannot be detected by TEC measurements. Another possible cause is the different scale size of EFIs identified by the GPS TEC fluctuations and the spread *F*. The GPS TEC fluctuations (ROTI) provide information on large-scale irregularities of electron density from several to several hundred kilometers. While the range-type spread *F* in ionograms is due to the reflection of radio waves from large-scale irregularities with structure as small as 3 m below or near the base of the *F* region [*Rastogi and Woodman*, 1978]. During geomagnetic quiet days of solar minimum, most EFIs are probably restricted around the *F* layer peak or below, which is far below the altitude of EFIs at solar maximum, when they often rise to over thousand kilometers and evolve into the topside plasma plumes, producing apparent in situ density depletions with an average altitude of more than 600 km [*Kil et al.*, 2009]. Considering the relatively low *F* layer height rise that precedes the postmidnight spread *F* of the solar minimum years (to be discussed below), we could expect that these spread *F* irregularities are unlikely to be associated with topside bubble structures. Rather, they could be bottomside irregularities without any significant plasma depletions so that the TEC values would not suffer fluctuations detectable by the GPS receivers. The occurrence discrepancy between GPS TEC fluctuations and ionosonde spread *F* might indicate that GPS TEC (ROTI) may be not a good parameter for studying the postmidnight EFIs at solar minimum, whereas it provides a measure of the irregularity occurrence resembling that of the spread *F* occurrence very much at solar maximum. The solar flux dependent effects can be readily noted also in other spread *F* characteristics and related parameters as follows.

[14] Over Kwajalein the spread *F* occurrences during solar minimum lag by 2 h behind those for the solar maximum years, which may be attributed to a difference in the evening vertical drift pattern (PRE) for the two epochs. The PRE is known to be controlled by thermospheric zonal wind (turning eastward before sunset) and the longitudinal/local time gradient in the Pederson and Hall conductivity across the terminator [e.g., *Farley et al.*, 1986; *Crain et al.*, 1993; *Su et al.*, 2009]. It has been shown by *Abdu et al.* [1992] that such gradient plays a major role in the onset time and amplitude of the prereversal drift, the PRE being largest at a given longitude when the sunset terminator and magnetic meridian are close to being aligned, a condition that is dependent on the magnetic declination angle. For the longitude of Kwajalein where the magnetic declination angle is positive (9° eastward), the most favorable alignment condition and therefore largest evening vertical drift and earlier *F* layer height rise occurs in June solstice, which explains the large growth rate of the R-T instability and the earlier onset and large occurrence rate of spread *F* also in this month. The PRE and *F* region heights decrease toward solar minimum [*Fejer et al.*, 1999], owing to the corresponding decreases of the equatorial zonal wind and conductivity gradient. This results in a small PRE and a possible delay in the zonal drift reversal. Thus we might expect that as a whole, a small PRE and the associated drift reversal delayed the spread *F* occurrence over Kwajalein during the June solstice of solar minimum as seen in Figure 6. In particular, small postreversal westward electric fields of solar minimum could lead to long-lived spread *F* events [*Hysell and Burcham*, 2002].

[15] Over Jicamarca, the June solstice spread *F* occurrences show a negative dependence with solar activity. The averaged prereversal vertical drift during the June solstice of solar maximum is less than 20 m s^{-1}, and even no PRE can be seen from the empirical drift model during solar minimum conditions [*Fejer et al.*, 1999]. Such a reduced prereversal drift in this longitude has been ascribed to the ionospheric electrodynamical effect resulting from the alignment of magnetic field line declination and sunset terminator as mentioned above [e.g., *Abdu et al.*, 1992; *Su et al.*, 2009]. In what follows we will discuss mainly the processes that can cause the generation of postmidnight EFIs at Peruvian sector, and the premidnight onset of EFIs at Pacific sector, during the June solstice of solar minimum.

4.1. Dependence on *F* Layer Height Increase

[16] In this section we present a statistical analysis on the behavior of the nighttime minimum virtual height (*h'F*) of the *F* layer and the *F*2 region critical frequency (f_oF_2) under spread *F* and non–spread *F* conditions, to investigate the possible dependence of the EFI occurrence (especially of the postmidnight hours) on increase in the *F* layer height. We divided the database into two categories: one of spread *F* occurrence and the other of nonoccurrence. Over Jicamarca, there are 35 nights with spread *F* (nine spread *F* events onset before 2200LT) and 25 nights without spread *F* during the two July months of 2007 and 2008. The top and bottom plots

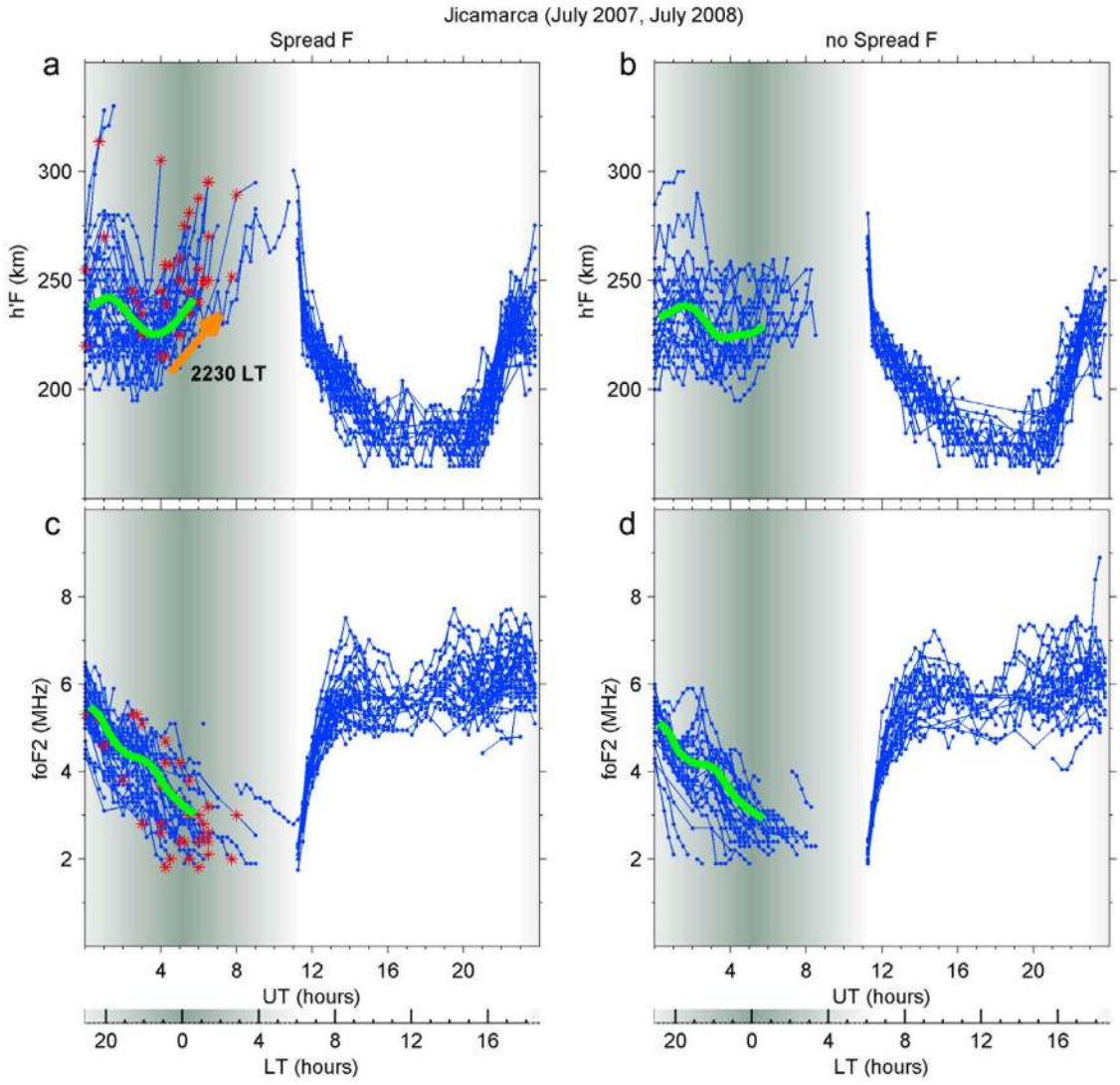

Figure 8. The behavior of minimum virtual height ($h'F$) of F layer and F_2 region critical frequency (f_oF_2) at nights (a and c) with spread F and (b and d) without spread F over Jicamarca during the two July months of 2007 and 2008. The bold green line shows the average value of scatterplots.

in Figure 8 represent variations of $h'F$ and f_oF_2 for the two types of nights, respectively. In Figures 8a and 8c the spread F onset times are marked by asterisks on each line, which often are interrupted owing to the spread F onset. After 0300 LT, the $h'F$ and f_oF_2 values are not available, owing to no-echo or spread F conditions. The bold line shows the average value of the scatterplots within 30 min smoothing window. In Figure 8a we may note that the mean $h'F$ increases during spread F nights as compared to the non–spread F nights. The increase begins at 2230 LT and attains a maximum value of about 250 km around 0100 LT with an uplift of about 20 km. The more striking feature is that many of the individual spread F events are preceded by substantial layer rise, indicating significant vertical drift as well. There is large dispersion in the onset times from one day to the other which accounts for a reduced mean vertical drift. On the non–spread F nights neither the average values of $h'F$ nor their individual values show any increase. This result indicates that the sudden postmidnight onset of EFIs occurs in close association with a substantial increase in F region height during the June solstice of solar minimum. The altitude increase favors the growth of instability owing to lower ion-neutral collision frequency. This feature is similar to the situation noticeable around the sunset period. It can be generally understood in terms of gravitational R-T instability, whose linear growth rate is inversely proportional to the ion-neutral collision frequency. These results highlight the fact that the elevated F region around midnight does lead to the development of postmidnight EFIs over Jicamarca. From the hourly averaged h_mF_2 values obtained from Ouagadougou in Africa, *Oyekola and Kolawole* [2010] investigated the vertical **E** × **B** drifts during solar maximum year 1989, an evening PRE peak was found located around 1900 LT during the June solstice. The usual evening PRE in the vertical drift, which is a manifestation of the enhancement of eastward electric field, peaks around 1800 LT and reverses to westward by 1900 LT over Jicamarca [e.g., *Fejer et al.*, 1999]. The cause of the altitude increase which takes place at much later time, around

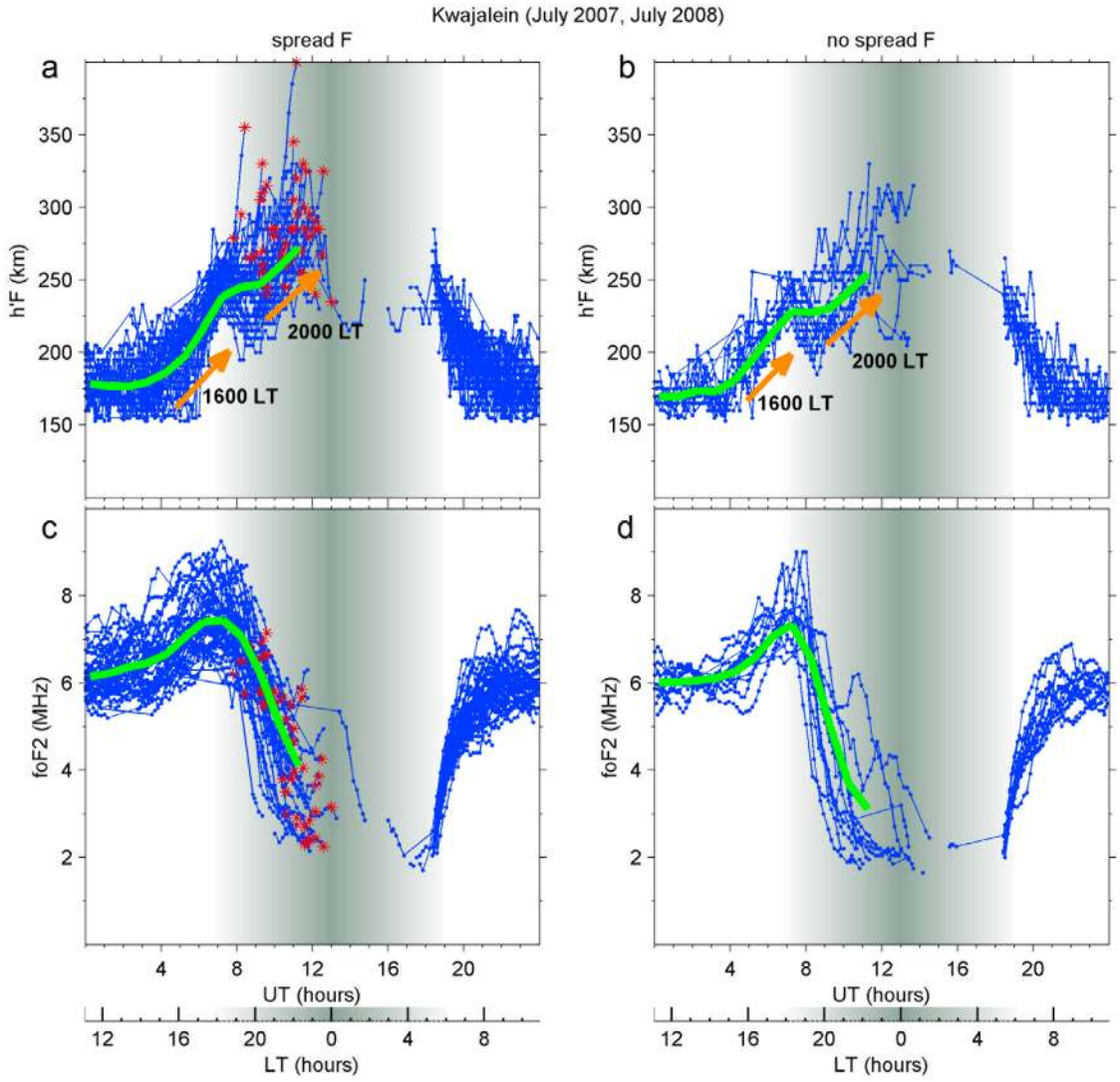

Figure 9. (a–d) Same as Figure 8 but for Kwajalein observations.

2230 LT (in the present data over Jicamarca), is not well understood. From previous studies we know that the major forces that can drive the ionosphere upward, besides the effects of electric field, are those caused by neutral winds and the horizontal advection of plasma. Furthermore, *Nicolls et al.* [2006] showed that recombination, instead of a zonal electric field reversal, can induce apparent midnight uplift at the magnetic equator provided that the downward vertical drift is sufficiently small. Further, model results show that during periods of low solar activity, the PRE is clearly dependent on the magnitude and phase of the semidiurnal tide [*Millward et al.*, 2001], and the June solstice postreversal westward electric field (or downward drift) is very small and starts to decrease after 2000 LT over Jicamarca [e.g., *Fejer et al.*, 1999; *Huang and Chen*, 2008]. Under these conditions the premidnight uplift of *F* layer over Jicamarca during the June solstice of solar minimum could be partly attributed to the above mentioned recombination effects, while some degree of tidal contribution should also be present. In Figures 8c and 8d, the f_oF_2 variations in spread *F* nights and non–spread *F* nights show similar characteristics, showing a decrease from 5 MHz to 3 MHz during the postsunset period with a slight enhancement centered around 2200 LT.

[17] Figure 9 shows the variations of $h'F$ and f_oF_2 over Kwajalein for spread *F* (Figures 9a and 9c) and non–spread *F* (Figures 9b and 9d) nights. During the two July months of 2007 and 2008, there are 46 nights with spread *F* and 14 nights without spread *F*. It is clear from Figure 9 that there is no striking difference in the pattern of variations in $h'F$ and f_oF_2 for the two sets of data, although, in general, the heights are higher for the spread *F* cases. The mean $h'F$ starts to increase at 1600 LT owing to the ionization decay associated with sunset, reaching close to 250 km at 1800 LT. The increase of $h'F$ then slows down till about 2000 LT but increases again by 2200 LT irrespective of whether spread *F* occurs or not. No clear indication of an enhanced prereversal vertical drift/zonal electric field is evident in the mean $h'F$ variation owing to the dominating recombination regime that is known to prevail below approximately 300 km [*Bittencourt and Abdu*, 1981]. However, the average height increase appears perceivably larger for the night of spread *F* (Figure 9a) than for the non–spread *F* nights. We may further

note that many individual cases of spread *F* onsets occur at the end of large height increases, which is very similar to the individual events noted also for Jicamarca. Just as over Jicamarca there is large day-to-day dispersion in the spread *F* onset times also over Kwajalein. Further, while there is significant number of spread *F* occurrences having their onsets during postmidnight hours over Jicamarca, for Kwajalein most events are initiated during premidnight hours and continue into postmidnight hours.

[18] This apparent connection between the height increase and spread *F* occurrence, especially in terms of individual events, might call attention to a possible dependence of spread *F* on *h′F* variation in June months which might also be longitude dependent. In Southeast Asian region, no *h′F* and f_oF_2 data were available for the present analysis to indicate whether spread *F* occurrence is associated with the height increase of *F* region, since the ionogram data obtained from Chumphon and Bac Lieu (in the form of printed pictures) did not permit determination of these parameters. However, the results presented for Ho Chi Minh City by *Hoang et al.* [2010] indicated that there is no apparent increase in *h′F* when spread *F* mainly occurred in the postmidnight hours. This can perhaps explain why the spread *F* occurrence rate in Southeast Asian longitude (30%) is lower than that of Kwajalein (80%). On the other hand, in the Indian sector, *Patra et al.* [2009] investigated the field-aligned irregularities (FAIs) as observed by the Gadanki radar and the spread *F* by ionosonde and found that the occurrence rate of the radar echo is higher than that of ionosonde spread *F* and simultaneous observations of *h′F* did not show any clear height rise. They speculated on the possibility of low-latitude Es activity (observed during premidnight hours) providing the necessary electric fields for the *F* region to be unstable. However, the postmidnight spread *F* observed at Kwajalein and Jicamarca does not seem to belong to the above situation.

4.2. Possible Explanations for the Observed Spread *F* Features

4.2.1. General Considerations

[19] On the basis of our current understanding derived from model and observational studies, we could suggest some explanation for the spread *F* features observed at these different longitudes. The primary causes for the ESF development can be stated briefly in terms of (1) the evening prereversal enhancement in zonal electric field (PRE) that drives the *F* layer to large heights, where the plasma instabilities develop by generalized gradient drift and/or Rayleigh-Taylor (R-T) mechanism leading to the formation of topside bubbles/field aligned depletions with associated irregularities that constitute the spread *F*; (2) density perturbation produced by gravity waves or TIDs for seeding the instability at the bottomside gradient region of a rising *F* layer; and (3) meridional/transequatorial winds modifying the field line integrated conductivities that control the nonlinear growth of the instability to form the bubbles.

[20] As regards to item 1, it is known from observations that the vertical drift due to the PRE should be at least 30 m s^{-1} for bubble irregularities to develop under medium to high solar flux conditions [see, e.g., *Fejer et al.*, 1999; *Abdu et al.*, 2006]. For low solar flux conditions it appears the bubble can develop even for smaller vertical drifts. Therefore the TEC fluctuations (ROTI) and the ionogram spread *F* events for the solar maximum conditions presented in Figures 3–5 could be generally associated with well developed bubbles (as the corresponding evening vertical drift is expected to be of the order of 30 m s^{-1} or more for this epoch). On the other hand, the spread *F* events presented in Figures 5–7 for solar minimum epoch are largely of bottomside irregularities, as the evening-postsunset *F* layer rise for these cases suggested very small vertical drifts, significantly smaller than 15 m s^{-1} that are inadequate for topside bubble development. Such inference can be made also from considerations on the transequatorial wind (of the above item 3) expected to be large in June months. *Maruyama* [1988] found that a transequatorial neutral wind tends to push the *F* layer in the Appleton anomaly upward along the magnetic field, and subsequently to push the conjugate *F* layer downward, thereby increasing the field line integrated conductivity which reduces the nonlinear growth of the instability by R-T mechanism. Consistent evidence for suppression of spread *F* by neutral winds is given by *Abdu et al.* [2006] and *Maruyama et al.* [2009]. Although the hemispheric asymmetry in solar UV heating (the thermal tides) is basically responsible for the transequatorial winds in solstitial months (in June months in the present study), there could be large day-to-day variability in such winds arising from other driving forces (such as gravity waves or planetary waves). While such variability could produce a corresponding variability in spread *F* bubble development as mentioned above, they may not have an impact on the bottomside spread *F* [see, e.g., *Abdu*, 1997] for which nonlinear instability growth (to topside) does not take place as a result of a low PRE/vertical drift intensity or even a background transequatorial wind. Another source of meridional winds in the equatorial region arises from the semipermanent equatorial midnight temperature maximum (MTM) [*Sastri et al.*, 1994]. During the summer solstice, the MTM is strongest and its characteristics are highly variable from day to day. From an investigation of multi-instruments observations, *Niranjan et al.* [2003] analyzed the seasonal variation of midnight spread *F* occurrence and MTM and found that the onset times of midnight spread *F* depended on the characteristics of MTM. However, the precise mechanism of the connection between the MTM associated winds and the spread *F* is unknown at present.

4.2.2. Triggering Effects of Perturbation Seed

[21] The presence of a seed perturbation (the above item 2) could play an important role in the generation of irregularities [*Abdu*, 2001]. There is evidence that equatorial spread *F* is not solely controlled by the *F* layer height rise; seeding by atmospheric gravity waves is beginning to emerge as an important contributor [*Tsunoda*, 2010b]. The possible importance of the prereversal vertical drift relative to the gravity wave intensity for seeding a spread *F* event has recently been discussed by *Abdu et al.* [2009b] and *Kherani et al.* [2009]. The gravity wave manifestation in the form of large-scale wave structure (LSWS) has been studied recently in detail mostly by ground-based radar, TEC receiver, and in situ satellite [e.g, *Singh et al.*, 1997; *Tsunoda*, 2005; *Thampi et al.*, 2009]. Earlier, from ionosonde observations, *Abdu et al.* [1981] showed that satellite traces preceded range-type equatorial spread *F* in the ionograms over Fortaleza. Such satellite traces in ionograms were recently identified as

signatures of LSWS [*Tsunoda*, 2008]. There appears to be two ways in which the LSWS can be connected with spread *F* development.

[22] 1. One example is presented in Figure 10, which shows a series of ionograms taken during the period 0800–0910 UT on 18 June 2005. Values of $h'F$ and f_oF_2 scaled from Kwajalein ionograms are noted in Figure 10. As shown in Figure 10a, $h'F$ was about 300 km and f_oF_2 was about 8 MHz. There is no evidence of satellite traces and spread *F* diffuse echoes. In the second ionogram at 0815 UT a satellite trace can be observed in the second hop (2F). The $h'F$ has increased to 319 km, but the f_oF_2 was still about 8 MHz. Another ionogram, taken 5 min later at 0820 UT, displays the satellite traces adjacent to the first hop (1F) with a more extended satellite trace at the 2F trace, with slight increase of $h'F$ up to 325 km. Similar features are presented in Figures 10b and 10d. After about 20 min, the bottomside range-type spread *F* appeared in ionogram at 0900 UT and became most disturbed at 0910 UT, as presented in Figure 10f. We may note here that the $h'F$ presented a small increase (by ~25 km from 0800 to 0820 UT) just preceding the appearance of the first satellite trace at 0820 UT. From the start of the first satellite trace it took ~40 min for the appearance of range spreading. In another case (not present here), similar variations of $h'F$ and f_oF_2 are observed, but no satellite trace/LSWS and spread *F* occurred. These results appear to suggest that the satellite traces indicative of LSWS can trigger the development of spread *F* and that the spread *F* occurrence is not necessarily associated with large/significant increases in the height of *F* region. From an investigation on day-to-day variability of spread *F*, *Tsunoda* [2005] pointed out that the presence of LSWS can modify the background conditions from three aspects: produce an additional polarization electric field, lead to a gradient in density that is steeper in crest than trough, and elevate the crest to higher altitude where ion-neutral collision frequency is smaller. These could favor the growth of small-scale irregularities by interchange instability. More recently, *Tsunoda et al.* [2010] presented some cases of equatorial spread *F* occurrence associated with LSWS even without a postsunset rise of the *F* layer. They suggested that atmospheric gravity waves are likely excited in localized regions of deep tropospheric convection, generated by mesoscale convective systems in the troposphere, and propagate up to the thermosphere, where they interact with the ionospheric plasma to induce perturbations in plasma density and produce LSWS. Using the lower atmospheric disturbances and equatorial spread *F* observations, *Tsunoda* [2010a] presents a tangible link between them. They found that the occurrences of equatorial spread *F* during the solstices are probably produced by enhanced seeding when the intertropical convergence zone (ITCZ, the most intense source of gravity waves) is located at the magnetic equator. During the June solstice, the mean ITCZ location over Pacific and Southeast Asia is situated near the magnetic dip equator. At times after sunset, the seeding may persist longer in the absence of postsunset rise of *F* layer, and the LSWS continue to grow. But the waveform can be distorted by contributions from gravity waves with other wavelength. If the *F* layer has been elevated to higher altitude, the vertical bulk-plasma transport and the acceleration of the zonal background neutral wind probably disrupt the seeding process. However, amplification of existing LSWS can probably continue through the interchange instability [*Tsunoda*, 2010b]. In the present study, although we found some cases of LSWS/satellite traces that are followed by spread *F* occurrence, not all spread *F* irregularities at Kwajalein could be associated with LSWS in its manifestation as satellite traces.

[23] 2. Some of the $h'F$ variations that end with the start of spread *F* in Figures 8 and 9 can in fact be interpreted as signatures of gravity wave induced LSWS. While a few of them do represent relatively larger height increase leading to instability growth possibly driven by vertical plasma drift, the others seems to be associated with instability growth driven by horizontal plasma drift. An $h'F$ oscillation, whose recording was interrupted with start of the spread *F* echoes, must be associated with *F* layer height undulations, which could produce downward bulges in bottomside density contours at the scale size of the gravity waves. The bulge formation could be enhanced by the R-T mechanism, and they are regions of horizontal density gradients that could lead to irregularity development through gradient drift instability mechanism in the presence of a zonal plasma drift (V_{east}) in neutral reference frame. *MacDougall et al.* [1998] proposed such a mechanism to explain the presunrise spread *F* occurrences that peaked during solstitial months over Fortaleza. The instability growth is given by $\gamma = V_{east} - U_{east}/L_h$, where U_{east} is the eastward neutral wind and L_h is the horizontal component of the density gradient arising from the tilt of the bottomside vertical gradient by the bulge (for details, see *MacDougall et al.* [1998]). For typical values of the parameters the growth time for the irregularity development was found to vary from 15 to 20 min over Fortaleza. A similar situation could apply also for the longitudes of Jicamarca and Kwajalein. This mechanism, which appears to be a viable one, could be proposed to explain, at least partly, the late night (after 2300 LT) as well as the postmidnight spread *F* over these stations.

[24] For both cases 1 and 2 discussed above, the presence of gravity waves is a basic requirement. Gravity waves could contribute to the development of EFI in at least two different ways. *Tsunoda* [2010c] proposed that zonally propagating gravity waves with their phase fronts aligned with magnetic meridian at the equator are most appropriate for the neutral-ion interaction to produce polarization electric field leading to instability development by R-T mechanism. This approach necessitates the gravity wave source to be located on the dip equatorial region in the longitude sector of the ESF occurrence. Regions of tropospheric convective activity associated with the ITZC are believed to be strong gravity waves sources. Therefore, on the basis of the correlation observed between the proximity of the ITCZ to the dip equator and the spread *F* occurrence enhancement in June solstitial months over Pacific stations, *Tsunoda* [2010c] substantiated his hypothesis on the need of a zonally propagating gravity waves for the instability seeding that could lead to EFI development. We believe this mechanism can be invoked to explain at least part of the late evening and postmidnight spread *F* occurrences over Kwajalein and Southeast Asian longitudes, although the occurrence rate is significantly less in the latter than in the former case.

[25] As another mechanism, we may consider the gravity waves propagating at an angle with the magnetic meridian. In this case a horizontally propagating wave, such as medium-

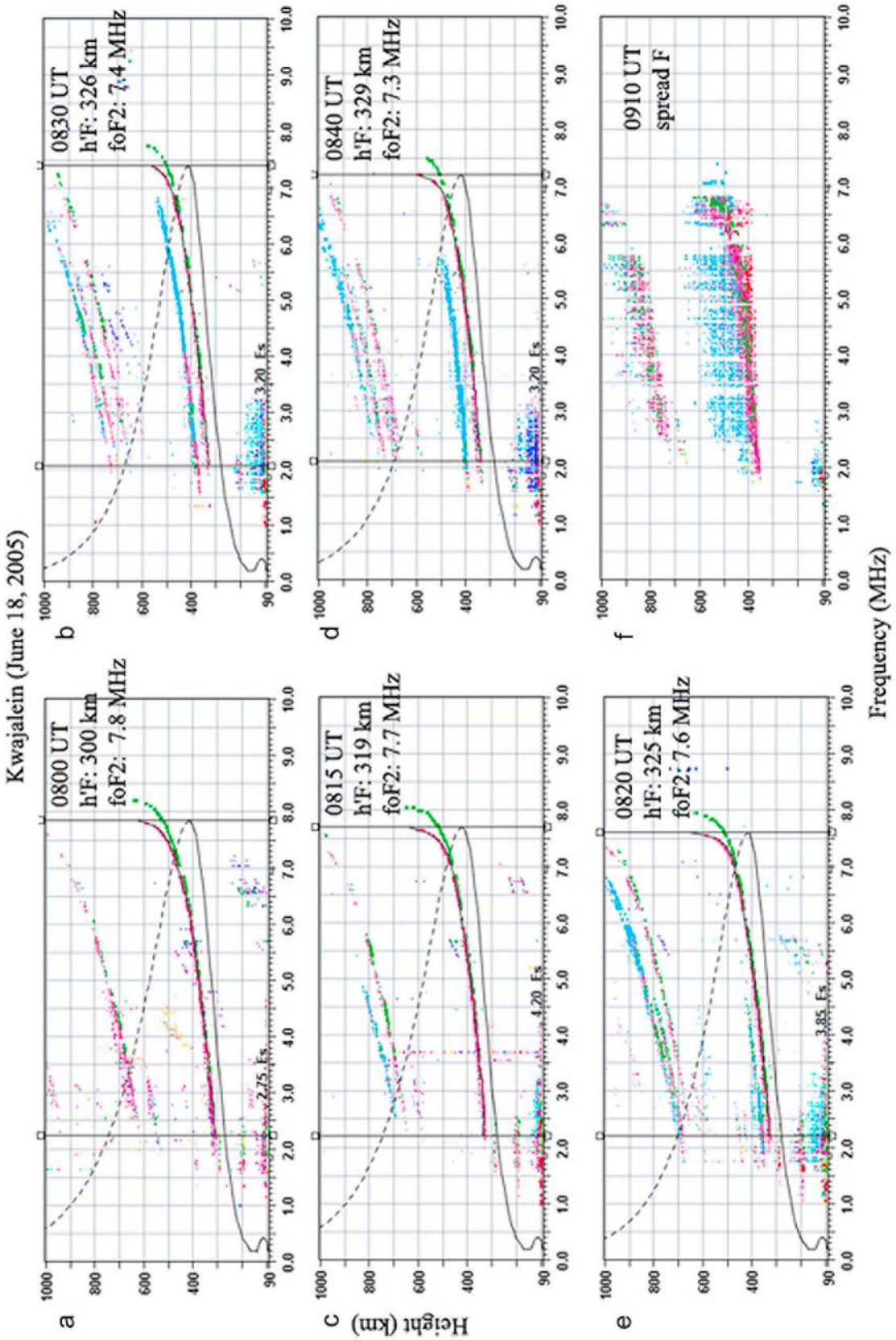

Figure 10. (a–f) Ionograms taken from Kwajalein showing that the satellite traces preceded RSF on 18 June 2005.

scale gravity wave (those driving the MSTIDs), making a significant angle with the magnetic meridian will have associated with it the perturbation winds contributing plasma motion along field lines. Oppositely moving plasma in the same field line could cause ionization convergence and plasma pileup contributing to bottomside bulge formation similar to that discussed earlier. Subsequent development of the bulge could lead to the irregularity growth through gradient drift mechanism discussed before. Such a mechanism does not require a gravity wave source located at the magnetic equator. This mechanism may well be operating for the postmidnight spread *F* development in June solstitial months over Jicamarca, since as shown in the OLR global map of *Tsunoda* [2010c, Figure 2], the expected source regions for gravity waves generation during this period is located mainly in the northern hemisphere of this longitude. In this way it looks possible to qualitatively explain most of the important features of the spread *F* occurrence in June solstitial months at the different longitude sectors analyzed in this paper.

5. Conclusion

[26] The occurrence statistics of postmidnight equatorial *F* region irregularities have been obtained from the ground-based GPS TEC and ionosonde data taken during the June solstice of 2000–2009. We analyzed the onset time and duration distribution of EFIs at different longitudes using both the TEC fluctuation index (ROTI) and the ionogram spread *F* records. It is found that at solar maximum, the EFIs occur mainly at African and Pacific sectors, with the peak occurrence rate located at postsunset. The postmidnight EFIs are mostly the continuation of premidnight EFIs, which was generated at postsunset hours owing to the prereversal vertical drift enhancements and continued for several hours until postmidnight. The decayed postmidnight EFIs are consistent with the in situ satellites observed dead bubbles. In the Peruvian region (~290°E), the solar maximum EFIs were totally suppressed. However, at solar minimum, the postmidnight EFIs were observed with an occurrence rate up to 50% around 0300 LT. The occurrence probability of postmidnight EFIs is apparently higher than that of postsunset. While during solar maximum the EFI observed by the TEC fluctuations (ROTI) and by the spread *F* corresponded well to each other, during solar minimum only the spread *F* showed large occurrence rates with 30%, 80%, and 50% at Southeast Asian, Pacific, and Peruvian longitudes, respectively, with ROTI rarely observed. During solar minimum a statistical analysis on the behavior of *h′F* at Jicamarca showed that there was an apparent increase of *h′F* starting around 2230 LT on spread *F* nights that was not present on non–spread *F* nights. It is thus concluded that the *F* layer height increase around midnight may be a requirement for the development of the postmidnight EFIs over Jicamarca. In the Pacific region, the solar minimum EFIs are mostly initiated at premidnight, around 2300 LT, and the postmidnight EFIs are the continuation of premidnight EFIs. The *h′F* variation over Kwajalein also showed a postsunset height increase beginning around 2000 LT that was larger on the spread *F* nights as compared to non–spread *F* nights. However, the height increases at both the longitudes do not appear to be of sufficient intensity to account by themselves for the midnight/postmidnight occurrence of EFIs. Other factors, such as the day-to-day variability of neutral wind and perturbation seed, could play important roles in the occurrence of EFIs in these longitudes. We have explained (qualitatively) the seed perturbation in the form of gravity waves, on the basis of their propagation conditions and their expected global occurrence pattern in June solstitial months (as available in published literature), to be consistent with the observed features of the spread *F* in the longitude sectors considered in the study.

[27] The current study of solar minimum EFIs indicates that the EFIs were predominantly initiated around midnight from gravity wave perturbations and survived for several hours until sunrise. The irregularities are generated first at the bottomside of *F* region and then tend to rise to higher altitude, with the peak occurrence rate centered at postmidnight, when the EFIs could be still active and growing. This possibly explains the C/NOFS observed polarization electric fields inside the postmidnight plasma bubbles [*Huang et al.*, 2010], since most EFIs are freshly generated at postmidnight during the June solstice of solar minimum.

[28] **Acknowledgments.** This research is supported by the Natural Science Foundation of China (41074113 and 40904038) and National Important Basic Research Project of China (2011CB811405). GPS TEC data and ionosonde data are provided from IGS, DIDB, and SEALION database. Assistance from the staff at Sanya station is much appreciated, in particular, Xiqing Hao, Zhaoguo Huang, and Zhijian Fu. Xinan Yue acknowledges support from the U.S. Air Force with funds awarded via the National Science Foundation under Cooperative Agreements AGS-0918398/CSA and AGS-0961147.

[29] Masaki Fujimoto thanks the reviewers for their assistance in evaluating this paper.

References

Abdu, M. A. (1997), Major phenomena of the equatorial ionosphere-thermosphere system under disturbed conditions, *J. Atmos. Sol. Terr. Phys.*, *59*, 1505–1519, doi:10.1016/S1364-6826(96)00152-6.

Abdu, M. A. (2001), Outstanding problems in the equatorial ionosphere-thermosphere electrodynamics relevant to spread *F*, *J. Atmos. Sol. Terr. Phys.*, *63*, 869–884.

Abdu, M. A., I. S. Batista, and J. A. Bittencourt (1981), Some characteristics of spread *F* at the magnetic equatorial station Fortaleza, *J. Geophys. Res.*, *86*, 6836–6842, doi:10.1029/JA086iA08p06836.

Abdu, M. A., I. S. Batista, and J. H. A. Sobral (1992), A new aspect of magnetic declination control of equatorial spread *F* and *F* region dynamo, *J. Geophys. Res.*, *97*, 14,897–14,904, doi:10.1029/92JA00826.

Abdu, M. A., K. N. Iyer, R. T. de Medeiros, I. S. Batista, and J. H. A. Sobral (2006), Thermospheric meridional wind control of equatorial spread *F* and evening prereversal electric field, *Geophys. Res. Lett.*, *33*, L07106, doi:10.1029/2005GL024835.

Abdu, M. A., I. S. Batista, B. W. Reinisch, J. R. de Souza, J. H. A. Sobral, T. R. Pedersen, A. F. Medeiros, N. J. Schuch, E. R. de Paula, and K. M. Groves (2009a), Conjugate Point Equatorial Experiment (COPEX) campaign in Brazil: Electrodynamics highlights on spread development conditions and day-to-day variability, *J. Geophys. Res.*, *114*, A04308, doi:10.1029/2008JA013749.

Abdu, M. A., E. Alam Kherani, I. S. Batista, E. R. de Paula, D. C. Fritts, and J. H. A. Sobral (2009b), Gravity wave initiation of equatorial spread F/plasma bubble irregularities based on observational data from the SpreadFEx campaign, *Ann. Geophys.*, *27*, 2607–2622, doi:10.5194/angeo-27-2607-2009.

Basu, Su., S. Basu, J. Huba, J. Krall, S. E. McDonald, J. J. Makela, E. S. Miller, S. Ray, and K. Groves (2009), Day-to-day variability of the equatorial ionization anomaly and scintillations at dusk observed by GUVI and modeling by SAMI3, *J. Geophys. Res.*, *114*, A04302, doi:10.1029/2008JA013899.

Bhattacharyya, A., S. Basu, K. M. Groves, C. E. Valladares, and R. Sheehan (2001), Dynamics of equatorial *F* region irregularities from

spaced receiver scintillation observations, *Geophys. Res. Lett.*, *28*, 119–122, doi:10.1029/2000GL012288.

Bittencourt, J., and M. Abdu (1981), A theoretical comparison between apparent and real vertical ionization drift velocities in the equatorial *F* region, *J. Geophys. Res.*, *86*(A4), 2451–2454.

Chen, W. S., C. C. Lee, J. Y. Liu, F. D. Chu, and B. W. Reinisch (2006), Digisonde spread *F* and GPS phase fluctuations in the equatorial ionosphere during solar maximum, *J. Geophys. Res.*, *111*, A12305, doi:10.1029/2006JA011688.

Crain, D., R. Heelis, G. Bailey, and A. Richmond (1993), Low-latitude plasma drifts from a simulation of the global atmospheric dynamo, *J. Geophys. Res.*, *98*, 6039–6046, doi:10.1029/92JA02196.

Farley, D., E. Bonelli, B. Fejer, and M. Larsen (1986), The prereversal enhancement of the zonal electric field in the equatorial ionosphere, *J. Geophys. Res.*, *91*(A12), 13,723–13,728.

Fejer, B. G., L. Scherliess, and E. R. de Paula (1999), Effects of the vertical plasma drift velocity on the generation and evolution of equatorial spread *F*, *J. Geophys. Res.*, *104*, 19,859–19,869, doi:10.1029/1999JA900271.

Hoang, T. L., M. A. Abdu, J. MacDougall, and I. S. Batista (2010), Longitudinal differences in the equatorial spread *F* characteristics between Vietnam and Brazil, *Adv. Space Res.*, *45*, 351–360, doi:10.1016/j.asr.2009.08.019.

Huang, C. M., and M. Q. Chen (2008), Formation of maximum electric potential at the geomagnetic equator by the disturbance dynamo, *J. Geophys. Res.*, *113*, A03301, doi:10.1029/2007JA012843.

Huang, C.-S., O. de La Beaujardiere, R. F. Pfaff, J. M. Retterer, P. A. Roddy, D. E. Hunton, Y.-J. Su, S.-Y. Su, and F. J. Rich (2010), Zonal drift of plasma particles inside equatorial plasma bubbles and its relation to the zonal drift of the bubble structure, *J. Geophys. Res.*, *115*, A07316, doi:10.1029/2010JA015324.

Huba, J. D., G. Joyce, and J. Krall (2008), Three-dimensional equatorial spread F modeling, *Geophys. Res. Lett.*, *35*, L10102, doi:10.1029/2008GL033509.

Hysell, D. L., and J. D. Burcham (2002), Long term studies of equatorial spread *F* using the JULIA radar at Jicamarca, *J. Atmos. Sol. Terr. Phys.*, *64*, 12–14, 1531–1543.

Kherani, E. A., M. A. Abdu, E. R. de Paula, D. C. Fritts, J. H. A. Sobral, and F. C. de Meneses Jr. (2009), The impact of gravity waves rising from convection in the lower atmosphere on the generation and nonlinear evolution of equatorial bubble, *Ann. Geophys.*, *27*, 1657–1668, doi:10.5194/angeo-27-1657-2009.

Kil, H., L. J. Paxton, and S.-J. Oh (2009), Global bubble distribution seen from ROCSAT-1 and its association with the evening prereversal enhancement, *J. Geophys. Res.*, *114*, A06307, doi:10.1029/2008JA013672.

King, G. A. (1970), Spread *F* on ionograms, *J. Atmos. Terr. Phys.*, *32*, 209–221, doi:10.1016/0021-9169(70)90192-3.

Lee, C. C., F. D. Chu, W. S. Chen, J. Y. Liu, S.-Y. Su, Y. A. Liou, and S. B. Yu (2009), Spread *F*, GPS phase fluctuations, and plasma bubbles near the crest of equatorial ionization anomaly during solar maximum, *J. Geophys. Res.*, *114*, A08302, doi:10.1029/2009JA014195.

Li, G., B. Ning, L. Liu, W. Wan, and J. Y. Liu (2009a), Effect of magnetic activity on plasma bubbles over equatorial and low-latitude regions in East Asia, *Ann. Geophys.*, *27*, 303–312, doi:10.5194/angeo-27-303-2009.

Li, G., B. Ning, B. Zhao, L. Liu, W. Wan, F. Ding, J. S. Xu, J. Y. Liu, and K. Yumoto (2009b), Characterizing the 10 November 2004 storm-time middle-latitude plasma bubble event in Southeast Asia using multi-instrument observations, *J. Geophys. Res.*, *114*, A07304, doi:10.1029/2009JA014057.

MacDougall, J., M. Abdu, P. Jayachandran, J.-F. Cecile, and I. Batista (1998), Presunrise spread *F* at Fortaleza, *J. Geophys. Res.*, *103*, 23,415–23,425, doi:10.1029/98JA01949.

Maruyama, T. (1988), A diagnostic model for equatorial spread *F*: 1. Model description and application to electric field and neutral wind effects, *J. Geophys. Res.*, *93*, 14,611–14,622, doi:10.1029/JA093iA12p14611.

Maruyama, T., S. Saito, M. Kawamura, K. Nozaki, J. Krall, and J. D. Huba (2009), Equinoctial asymmetry of a low-latitude ionosphere-thermosphere system and equatorial irregularities: Evidence for meridional wind control, *Ann. Geophys.*, *27*, 2027–2034, doi:10.5194/angeo-27-2027-2009.

Millward, G., I. Müller-Wodarg, A. Aylward, T. Fuller-Rowell, A. Richmond, and R. Moffett (2001), An investigation into the influence of tidal forcing on *F* region equatorial vertical ion drift using a global ionosphere-thermosphere model with coupled electrodynamics, *J. Geophys. Res.*, *106*, 24,733–24,744, doi:10.1029/2000JA000342.

Nicolls, M. J., M. C. Kelley, M. N. Vlasov, Y. Sahai, J. L. Chau, D. L. Hysell, P. R. Fagundes, F. Becker-Guedes, and W. L. C. Lima (2006), Observations and modeling of post-midnight uplifts near the magnetic equator, *Ann. Geophys.*, *24*, 1317–1331, doi:10.5194/angeo-24-1317-2006.

Niranjan, K., P. S. Brahmanandam, P. Ramakrishna Rao, G. Uma, D. S. V. V. D. Prasad, and P. V. S. Rama Rao (2003), Post midnight spread-F occurrence over Waltair (17.7°N, 83.3°E) during low and ascending phases of solar activity, *Ann. Geophys.*, *21*, 745–750, doi:10.5194/angeo-21-745-2003.

Nishioka, M., A. Saito, and T. Tsugawa (2008), Occurrence characteristics of plasma bubble derived from global ground-based GPS receiver networks, *J. Geophys. Res.*, *113*, A05301, doi:10.1029/2007JA012605.

Oyekola, O. S. (2009), A study of evolution and suppression parameters of equatorial postsunset plasma instability, *Ann. Geophys.*, *27*, 297–301, doi:10.5194/angeo-27-297-2009.

Oyekola, O. S., and L. B. Kolawole (2010), Equatorial vertical E × B drift velocities inferred from ionosonde measurements over Ouagadougou and the IRI-2007 vertical ion drift model, *Adv. Space Res.*, *46*, 604–612, doi:10.1016/j.asr.2010.04.003.

Oyekola, O. S., A. Ojo, J. Akinrimisi, and E. R. dePaula (2007), Seasonal and solar cycle variability in *F*-region vertical plasma drifts over Ouagadougou, *J. Geophys. Res.*, *112*, A12306, doi:10.1029/2007JA012560.

Patra, A. K., D. V. Phanikumar, and T. K. Pant (2009), Gadanki radar observations of *F* region field-aligned irregularities during June solstice of solar minimum: First results and preliminary analysis, *J. Geophys. Res.*, *114*, A12305, doi:10.1029/2009JA014437.

Pi, X., A. J. Mannucci, U. J. Lindqwister, and C. M. Ho (1997), Monitoring of global ionospheric irregularities using the worldwide GPS network, *Geophys. Res. Lett.*, *24*, 2283–2286, doi:10.1029/97GL02273.

Rastogi, R. G., and R. F. Woodman (1978), VHF radio wave scattering due to range and frequency types of equatorial spread-*F*, *J. Atmos. Terr. Phys.*, *40*, 485–489, doi:10.1016/0021-9169(78)90182-4.

Reinisch, B. W., I. A. Galkin, G. Khmyrov, A. Kozlov, and D. F. Kitrosser (2004), Automated collection and dissemination of ionospheric data from the Digisonde network, *Adv. Radio Sci.*, *2*, 241–247, doi:10.5194/ars-2-241-2004.

Sastri, J. H. (1999), Letter to the Editor: Post-midnight onset of spread-*F* at Kodaikanal during the June solstice of solar minimum, *Ann. Geophys.*, *17*, 1111–1115, doi:10.1007/s00585-999-1111-4.

Sastri, J. H., B. S. Murthy, and K. Sasidharan (1979), Range and frequency spread-*F* at Kodaikanal, *Ann. Geophys.*, *35*, 153–158.

Sastri, J. H., H. N. Ranganath Rao, V. V. Somayajulu, and H. Chandra (1994), Thermospheric meridional neutral winds associated with equatorial midnight temperature maximum (MTM), *Geophys. Res. Lett.*, *21*, 825–828, doi:10.1029/93GL03009.

Singh, S., F. Johnson, and R. Power (1997), Gravity wave seeding of equatorial plasma bubbles, *J. Geophys. Res.*, *102*, 7399–7410, doi:10.1029/96JA03998.

Sripathi, S., S. Bose, A. K. Patra, T. K. Pant, B. Kakad, and A. Bhattacharyya (2008), Simultaneous observations of ESF irregularities over Indian region using radar and GPS, *Ann. Geophys.*, *26*, 3197–3213, doi:10.5194/angeo-26-3197-2008.

Su, S.-Y., C. K. Chao, and C. H. Liu (2009), Cause of different local time distribution in the postsunset equatorial ionospheric irregularity occurrences between June and December solstices, *J. Geophys. Res.*, *114*, A04321, doi:10.1029/2008JA013858.

Subbarao, K. S. V., and B. V. Krishnamurthy (1994), Seasonal variations of equatorial spread-*F*, *Ann. Geophys.*, *12*, 33–39.

Sultan, P. J. (1996), Linear theory and modeling of the Rayleigh-Taylor instability leading to the occurrence of equatorial spread *F*, *J. Geophys. Res.*, *101*, 26,875–26,891, doi:10.1029/96JA00682.

Thampi, S. V., M. Yamamoto, R. T. Tsunoda, Y. Otsuka, T. Tsugawa, J. Uemoto, and M. Ishii (2009), First observations of large-scale wave structure and equatorial spread *F* using CERTO radio beacon on the C/NOFS satellite, *Geophys. Res. Lett.*, *36*, L18111, doi:10.1029/2009GL039887.

Tsunoda, R. T. (2005), On the enigma of day-to-day variability in equatorial spread *F*, *Geophys. Res. Lett.*, *32*, L08103, doi:10.1029/2005GL022512.

Tsunoda, R. T. (2008), Satellite traces: An ionogram signature for large-scale wave structure and a precursor for equatorial spread *F*, *Geophys. Res. Lett.*, *35*, L20110, doi:10.1029/2008GL035706.

Tsunoda, R. T. (2010a), On seeding equatorial spread *F* during solstices, *Geophys. Res. Lett.*, *37*, L05102, doi:10.1029/2010GL042576.

Tsunoda, R. T. (2010b), On seeding equatorial spread *F*: Circular gravity waves, *Geophys. Res. Lett.*, *37*, L10104, doi:10.1029/2010GL043422.

Tsunoda, R. T. (2010c), On equatorial spread *F*: Establishing a seeding hypothesis, *J. Geophys. Res.*, *115*, A12303, doi:10.1029/2010JA015564.

Tsunoda, R. T., D. M. Bubenik, S. V. Thampi, and M. Yamamoto (2010), On large-scale wave structure and equatorial spread *F* without a post-

sunset rise of the *F* layer, *Geophys. Res. Lett.*, *37*, L07105, doi:10.1029/2009GL042357.

Woodman, R. F., and C. LaHoz (1976), Radar observations of *F* region equatorial irregularities, *J. Geophys. Res.*, *81*, 5447–5466, doi:10.1029/JA081i031p05447.

M. A. Abdu, Divisão de Aeronomia, Instituto Nacional de Pesquisas Espaciais, Avenida dos Astronautas, 1758, Jardim da Granja, São José dos Campos, São Paulo CEP 12227-010, Brazil.

L. Hu, G. Li, L. Liu, B. Ning, and W. Wan, Beijing National Observatory of Space Environment, Institute of Geology and Geophysics, Chinese Academy of Sciences, Beijing 100029, China. (gzlee@mail.iggcas.ac.cn)

X. Yue, University Corporation for Atmospheric Research, Boulder, CO 80307, USA.